Electronic structure of MnO studied by angle-resolved and resonant photoemission

Robert J. Lad* and Victor E. Henrich
Applied Physics, Yale University, P.O. Box 2157, New Haven, Connecticut 06520
(Received 4 April 1988)

Results are reported from angle-integrated, angle-resolved, and resonant photoemission measurements on cleaved MnO single crystals using synchrotron radiation. Normal-emission spectra from a cleaved (100) surface indicate that the relative dispersion of Mn $3d$ states in the valence band is less than ± 0.1 eV along $\Gamma-\Delta-X$ in the Brillouin zone, which supports the view of highly localized $3d$ electrons on the Mn^{2+} cations. The results of polarization-dependent and off-normal-emission measurements are also consistent with a localized Mn $3d$ orbital picture. To explain the presence of satellite photoemission peaks, a hybridization between Mn $3d$ and O $2p$ valence states must be invoked. The degree of hybridization is evident from resonant-photoemission measurements at the Mn $3p \rightarrow 3d$ absorption threshold. The antiresonant behavior of the $3d$-derived states near the top of the valence band in constant-initial-state spectra suggests that MnO is a charge transfer rather than a Mott insulator. The experimental results are discussed in the context of recent cluster and band theories which have been proposed to explain the insulating nature and electronic structure of MnO.

I. INTRODUCTION

The insulating nature of MnO and the other antiferromagnetic transition-metal monoxides (i.e., FeO, CoO, and NiO) was originally explained by the Mott-Hubbard theory,[1] which asserts that the d-d intra-atomic Coulomb energy in these materials is much greater than the $3d$ bandwidth, thereby giving rise to a gap between the filled and empty states in the $3d$ band. Although it has been generally recognized that electron-electron correlation effects are of central importance in explaining the electronic structure of these materials, there has recently been controversy concerning not only the magnitude of the Coulomb interaction but, also more fundamentally, whether the insulating gap is of cation $3d \rightarrow$cation $3d$ or of anion $2p \rightarrow$cation $3d$ character.[2-7] Calculations of the electronic properties of the rocksalt monoxides have been performed in the framework of two seemingly contradictory approaches: a single-particle band theory[8-12] and a more localized electron picture that includes configuration interactions between hybridized $3d$ and ligand orbitals.[7,13,14] Both methods seem to provide results that are in agreement with many of the experimental observations.

One of the earliest calculations of the nonmagnetic energy band structure of MnO by Mattheiss[8] incorrectly predicted a metallic ground state. By including antiferromagnetic interactions, Wilson[9] and Andersen *et al.*[10] were able to produce a gap within the $3d$ band although their calculations were not self-consistent. Recently, Oguchi *et al.*[11] performed self-consistent augmented-spherical-wave band calculations which included a treatment of exchange and correlation within a local-spin-density formalism. Their results show that the band structure is strongly dependent upon magnetic ordering and, in particular, that MnO is an insulator when the antiferromagnetic ordering is along the [111] direction, as is observed experimentally.[15] Their calculations also indicate that an insulating gap is retained when MnO is in the paramagnetic state at room temperature. The important result of their work is that a conventional band gap can be created within the $3d$ band of MnO without explicitly utilizing the Mott insulator concept.

A fundamentally different view of the electronic structure of MnO and the other rocksalt transition-metal monoxides is based on highly localized electron behavior, and calculations have been performed using cluster theories. Fujimori *et al.*[13] successfully simulated the valence band photoemission spectrum of NiO by considering configuration interactions (CI's) within a $(NiO_6)^{10-}$ octahedrally coordinated cluster. Hybridization between $3d$ and ligand orbitals was taken into account, and the relative intensities of the photoemission final states were calculated for different configurations of the transition-metal ion, including the atomic multiplet structure. The most intense features in the valence band photoemission spectrum were found to be associated with ligand-to-metal charge transfer screening of the d holes. Based upon these results, the insulating gap in NiO is interpreted as a ligand $2p \rightarrow$metal $3d$ charge transfer gap rather than the traditional $3d \rightarrow 3d$ Mott-Hubbard gap.[13] For MnO, the CI cluster calculation by Fujimori[14] suggests that the charge transfer energy may be about the same magnitude as the Mott-Hubbard gap. Zaanen *et al.*[7] have expanded the cluster model to include an anion valence-band width with a corresponding delocalized hole by treating the cation as an isolated impurity in an anion lattice. Their results provide a generalized theory for describing the electronic structure of the transition metal monoxides, which is based on the relative magnitudes of the charge transfer and Mott-Hubbard gaps.

MnO is conceptually the simplest of the rocksalt monoxides since the large atomic exchange splitting of the $Mn^{2+}(3d^5)$ ion separates the $3d$ level into occupied

spin-up and empty spin-down components. However, most experimental studies have been performed on NiO rather than MnO primarily because it is easier to grow in single crystal form. To date, the few experiments that have probed the electronic structure of MnO have relied on optical reflectance[16,17] and absorption[18] methods, which have revealed a gap of 1.8 eV within the $3d$ band and an absorption edge of 3.8 eV. Photoemission from the MnO valence band was first reported by Eastman and Freeouf[19] and is discussed further in Sec. III.

In this paper we report the results of angle-integrated, angle-resolved, and resonant photoemission experiments on cleaved single crystals of MnO using synchrotron radiation. The results are interpreted in the context of the proposed theories for the electronic structure. All of the experiments were performed at room temperature (well above the Néel temperature of 122 K) where MnO is in the paramagnetic state. Section II describes the sample characteristics and measurement techniques. Section III presents angle-integrated valence band spectra and compares the data to the predictions of band theory and cluster models. The results of angle-resolved measurements are presented in Sec. IV, including some data showing the effects of photon polarization. Section V discusses core level and valence band photoemission satellites. Section VI concentrates on the resonant enhancement of the $3d$ states near the $3p$-$3d$ absorption threshold. Finally, Sec. VII discusses the experimental results in terms of both the itinerant and the localized electron points of view that have been used to describe the electronic structure and insulating nature of MnO.

II. EXPERIMENT

The valence-band photoemission experiments were performed on beamline U14 at the National Synchrotron Light Source (NSLS) at Brookhaven National Laboratory using a plane grating monochromator with photon energies between 30 and 120 eV. Angle-resolved photoemission spectra were measured with a Vacuum Generators Model 424 hemispherical analyzer, operating with a 15 eV pass energy and at $\pm 2°$ angular resolution. A Physical Electronics 15-255G double pass cylindrical mirror analyzer (CMA), also employing a 15 eV pass energy, was used for angle-integrated measurements. The energy resolution in the measured spectra, determined primarily by the monochromator, ranged from about 0.2 eV at $h\nu = 30$ eV to 0.5 eV at $h\nu = 100$ eV. Core level photoemission spectra was measured in a multiple technique surface analysis system at Yale using an Al-anode x-ray source ($h\nu = 1486.6$ eV) and a double pass CMA, with an overall resolution of about 0.8 eV. Some valence band photoemission spectra were also measured at Yale using unpolarized He I and He II radiation generated by a dc discharge lamp.

Single crystal MnO samples, obtained from Crystal Tec (Grenoble, France), exhibited high quality Laue x-ray diffraction patterns from the rocksalt structure. X-ray diffractometer analysis of a powder sample made from part of a single crystal revealed that the sample contained approximately 7 at. % of α-Mn_3O_4; the presence of this second phase did not markedly affect the quality of the monocrystalline MnO phase and is too small to be discernible in the photoemission spectra. Cleavage rods about 4 mm $\times$ 4 mm in cross section were cut from a single crystal boule, with the [100] direction oriented parallel to the rod axis. Because of the high bulk resistivity of MnO at room temperature ($\simeq 10^9\ \Omega$ cm),[20] the rods were coated with $\simeq \frac{1}{2}\ \mu$m of a Pd-Au alloy to minimize charging effects by enhancing the electrical conductivity from the cleavage face to the spectrometer ground. The samples were cleaved *in situ* to expose a (100) surface; the pressure in the spectrometer vacuum chamber remained below 2×10^{-10} Torr throughout the measurements.

In spite of the insulating nature of MnO, a somewhat diffuse (1×1) LEED pattern could be observed from a cleaved surface for incident electron beam energies > 250 eV. At lower energies, charging precluded the observation of any pattern; a similar LEED charging threshold for MnO(100) has been reported by Prutton *et al.*[21] During photoemission, a small amount of steady-state charging was present. It did not distort the measure spectrum, but it did prevent a precise determination of the Fermi level. Therefore, all of the valence-band spectra presented in this study are referenced in energy to the $t_{2g\uparrow}(^5T_2)$ peak so that relative comparisons can be made.

Normal and off-normal emission electron energy distribution curves (EDC's) were measured with the angle-resolved hemispherical detector, employing several different incident photon polarizations. In addition, constant-initial-state (CIS) and constant-final-state (CFS) spectra were taken in the angle-integrated mode using the CMA; care was taken to correctly account for the background as discussed in Sec. VI. Total electron yield spectra were simply determined by monitoring the sample current to ground. For each spectrum in which the photon energy was varied, the photocurrent of a Ni diode monitor was used to correct for the variation in light intensity from the monochromator.

III. VALENCE-BAND PHOTOEMISSION

Valence-band photoemission spectra measured from cleaved MnO(100) are shown in Fig. 1 along with the valence-band structure predicted by band theory[11] and cluster calculations.[14] The experimental spectra in Fig. 1(a) were obtained using unpolarized He I (21.2 eV) and He II (40.8 eV) radiation. As mentioned above, the spectra are referenced in energy to the $^5T_2$ peak. The main spectral features are in good agreement with those published by Eastman and Freeouf,[19] who interpreted the valence band spectrum simply in terms of ligand field theory. As will become apparent, the valence band consists of overlapping O $2p$ and Mn $3d$ states; but, as a first approach, hybridization between the cation and ligand states can be neglected, and the main photoemission features can be assigned to localized $3d^{n-1}$ final states within a ligand field theory description. The validity of this assumption will be addressed in Secs. V and VII.

In a ligand field picture the bonding is assumed to be totally ionic, and the valence band is derived from O^{2-} anions in a closed-shell $2p^6$ configuration and Mn^{2+} cat-

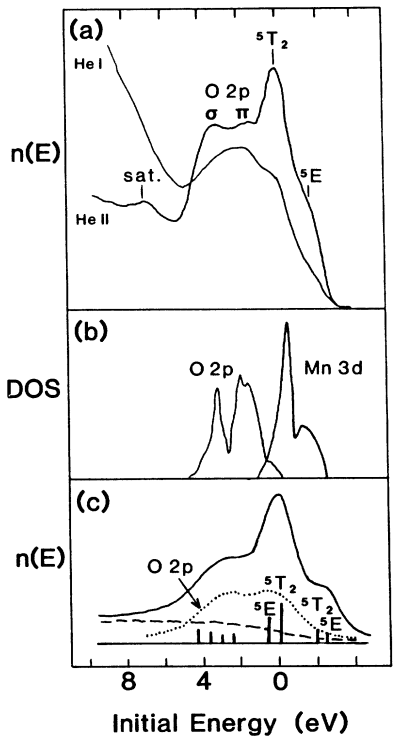

FIG. 1. Valence-band structure of paramagnetic MnO. (a) Angle-integrated photoemission spectra measured with He I and He II radiation. (b) Occupied density of states (DOS) calculated from one-electron band theory (Ref. 11), with the Mn $3d$ states shifted towards the O $2p$ states by about 1.1 eV. (c) Simulated photoemission spectrum from CI calculations for a $(MnO_6)^{10-}$ cluster (Ref. 14).

ions in a $3d^5$ configuration; the relevant orbitals are shown schematically in Fig. 2. The ground-state $Mn^{2+}(3d^5)$ ion has $^6A_1$ symmetry, and the degeneracy of the $3d$ orbitals is split by the octahedral field of O^{2-} anions into a $(t_{2g\uparrow})^3(e_{g\uparrow})^2$ configuration. The e_g components correspond to the d_{z^2} and $d_{x^2-y^2}$ orbitals which

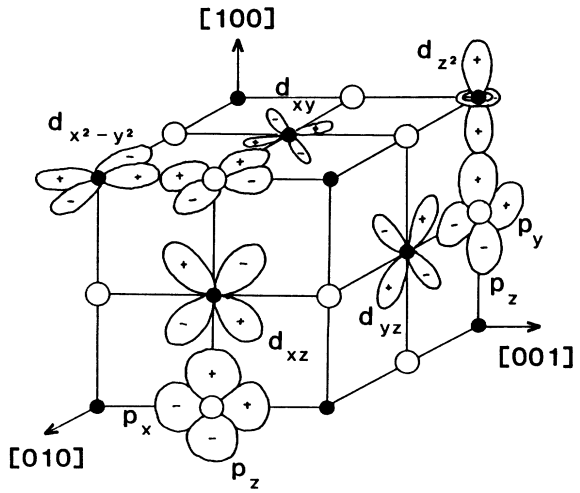

FIG. 2. Schematic diagram showing some of the Mn $3d$ and O $2p$ orbitals in a ligand field picture for MnO.

are σ bonded to the O^{2-} anions, and the remaining $3d$ orbitals make up the t_{2g} components which are π bonded to the O^{2-} anions.[22] The $3d^4$ final states of the photoemission process, $^5T_2$ and ^5E, results from $t_{2g\uparrow}$ and $e_{g\uparrow}$ excitation, respectively,[23] and are visible near the top of the valence band in Fig. 1(a). From the separation of these $3d$ states, the crystal field splitting is estimated to be about 1.8 eV. The predominately O $2p$ derived region in the valence band is located between 1 and 5 eV, and we tentatively separate the emission into components arising from σ and π bonding orbitals. The feature located around 7 eV cannot be explained using a simple ligand field model; its origin will be discussed in Sec. V.

Figure 1(b) shows the occupied density of states (DOS) for paramagnetic MnO calculated using one electron band theory by Oguchi *et al.*[11] To obtain good agreement with the photoemission experiment, the calculated Mn $3d$ band was shifted towards the O $2p$ band by about 1.1 eV. Approximately a 2 eV discrepancy in the anion p to cation d separation between DOS calculations and the experimental UPS spectrum has also been noted for antiferromagnetic NiO by Kübler and Williams;[24] they attribute the difference to be an energy shift of the $3d$ states due to the creation of a d hole during the photoemission process. For paramagnetic MnO, Ojala and Terakura[3] quote the shift to be only 1 eV when comparing the DOS calculations to data in Ref. 19, and they postulate that this smaller d band shift in MnO compared to NiO is associated with enhanced d-d hopping in the paramagnetic state. From a comparison between the DOS calculations and Fig. 1(a), our estimate for the energy shift in MnO is about 1.1 eV.

Using CI theory and a $(MnO_6)^{10-}$ cluster, Fujimori[14] has simulated the measured valence band photoemission spectrum for MnO as shown in Fig. 1(c). The relative magnitudes of the calculated final states, which include different configuration components, are indicated by vertical lines. The spectral line shape was obtained by broadening each of the lines with Gaussian functions and convoluting them with an O $2p$ emission and inelastic background to obtain a reasonable fit. The calculations indicate that the photoemission spectrum contains overlapping O $2p$ and Mn $3d$ states, and that the $3d$ contribution is made up of both $3d^4$ and $3d^5\underline{L}$ final states, where $\underline{L}$ represents a ligand hole formed by ligand-to-metal charge transfer.

Clearly both the band and cluster calculations appear to provide valid interpretations of the angle-integrated valence band photoemission spectra. The new experimental data that we present in this paper probe the valence band in more detail by using angle-resolved and resonant photoemission.

IV. ANGLE-RESOLVED PHOTOEMISSION

A. Normal emission

Angle-resolved photoemission is a well-established experimental technique that has been used to determine bulk energy band dispersions in many metals and semiconductors.[25] However, very few angle-resolved measurements have been performed on transition-metal ox-

ides since the valence-band features of these oxides are generally quite broad and complex, making dispersion measurements difficult. Band mapping has only recently been attempted for $SrTiO_3$,[26] Ti_2O_3,[27] V_2O_3,[27] and Fe_3O_4.[28,29] Nonetheless, we have performed normal emission experiments to observe the energy dispersion of states within the valence band of MnO, with the aim of determining whether a one electron band theory is appropriate for describing the electronic structure of the valence region.

Normal emission experiments are usually interpreted within a direct transition model using free-electron-like final states. In this approximation, the initial state wave vector of an electron in the solid ($k_\perp$) can be related to the kinetic energy of the electron measured in vacuum (E) using the relation[25]

$$k_\perp = \left[\frac{2m}{\hbar^2}(E+V_0)\right]^{1/2}, \quad (1)$$

where V_0 is a constant inner potential. A normal emission experiment from MnO(100) probes the [100] direction in k space, and $k_\perp$ is traversed completely from Γ to X in the second Brillouin zone for photon energies between $30 \leq h\nu \leq 80$ eV.

Figure 3 shows normal emission data from cleaved MnO(100) measured for two different polarizations of the incident photon beam. For an incident angle α of 80° with respect to the (100) surface normal, the electric vector of the linearly polarized radiation is nearly perpendicular to the sample surface, corresponding to predominately p polarization; for the 45° geometry, the incident radiation is of mixed sp polarization. The effects of changing the polarization are discussed in Sec. IV B. Each spectrum is normalized to a constant integrated area of the valence band above an integral inelastic background. (The backgrounnd at each point was assumed to be proportional to the total integrated intensity at higher kinetic energies.) The energy scale is adjusted so as to align the $t_{2g\uparrow}$ emission peak in all of the spectra. With this normalization procedure, only dispersions relative to the $t_{2g\uparrow}$ emission could be measured. However, this limitation is not significant in analyzing the main results.

By fitting the top of the valence band in Figs. 3(a) and 3(b) to the sum of two Gaussians (corresponding to the $e_{g\uparrow}$ and $t_{2g\uparrow}$ emission) it was found that these Mn-derived states, separated by 1.8 eV, do not disperse more than ±0.1 eV with respect to each other across the entire Brillouin zone. Contrarily, band-structure calculations[9,10] for MnO predict that the relative dispersion between $t_{2g\uparrow}$ and $e_{g\uparrow}$ emission should be at least 0.4 eV for $\Gamma-\Delta-X$ in the Brillouin zone. We believe that the observed lack of dispersion is strong evidence for localized $3d$ electrons. In the O $2p$ region located between 1 and 5 eV, some dispersion is evident, as suggested by the dashed lines in Figs. 3(a) and 3(b). However, we are unable to do band mapping of these states within the Brillouin zone because the broad and complex nature of the peaks prevents an

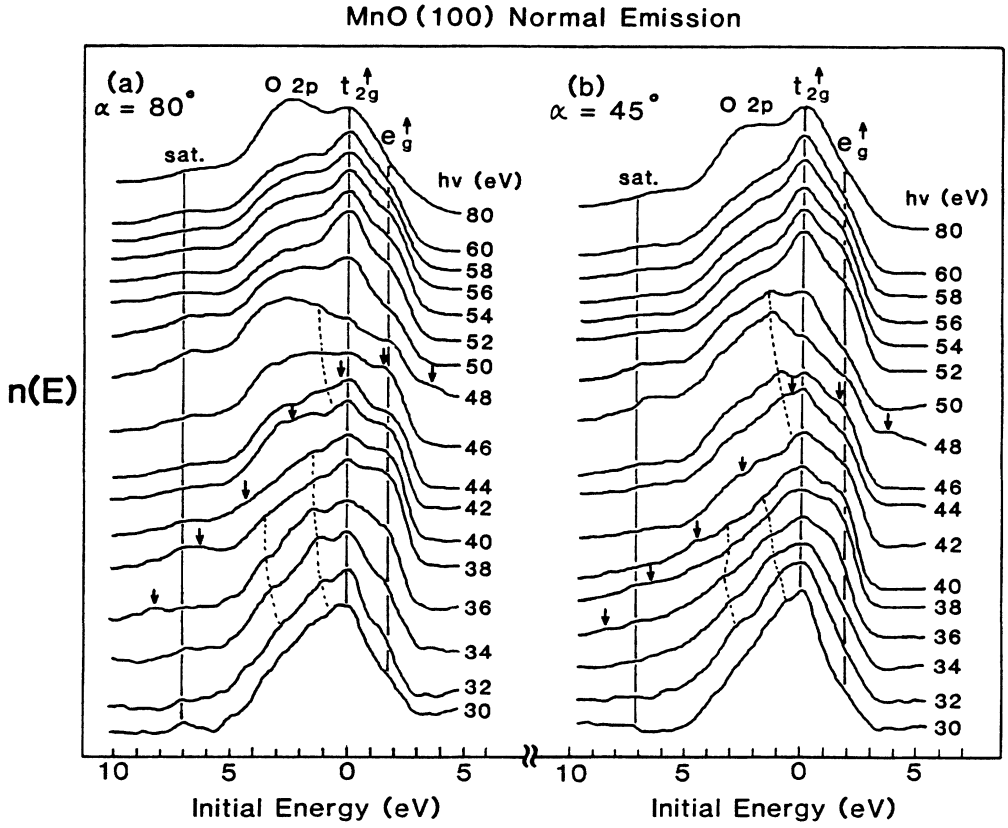

FIG. 3. Normal emission spectra from cleaved MnO(100) for photon energies from 30 to 80 eV with (a) nearly p polarization ($\alpha=80°$) and (b) mixed sp polarization ($\alpha=45°$).

unambiguous assignment of peak positions. The presence of dispersion for the O $2p$ states is nevertheless noteworthy, and it supports the model proposed by Zaanen *et al.*[7] which considers both highly localized cation $3d$ states and a dispersional anion band formed by ligand-ligand hybridization.

Another feature that is visible in the normal emission spectra is a satellite peak located near 7 eV, which shows an apparent enhancement in intensity between $48 \leq h\nu \leq 52$ eV; the origin and behavior of this satellite will be discussed in detail in Sec. VI. As pointed out by Kato *et al.*,[30] the $M_{23}M_{45}M_{45}$ super-Coster-Kronig (sCK) Auger peak that occurs at constant kinetic energy within this energy range can be mistaken for a satellite in valence band spectra of transition metals and their compounds. Although the sCK peak has been observed in MnP,[31] its intensity appears to be very weak in MnO and is not visible in any of the spectra. A small peak having constant kinetic energy (denoted by the arrows in Fig. 3) is observed for $36 \leq h\nu \leq 48$ eV; it is due to Mn $3p$ emission generated by second-order light from the monochromator.

B. Polarization dependence

Normal emission valence band spectra measured with nearly s polarization ($\alpha = 30°$) and p polarization ($\alpha = 80°$) of the incident light with respect to the MnO(100) surface are compared at several photon energies in Fig. 4. (The geometry of the experimental arrangement did not allow for a total s- or p-polarization condition.) Each of the spectra is normalized to a constant integrated area above an integral inelastic background so that the relative intensities of the valence band features can be observed as a function of the polarization of the incident light.

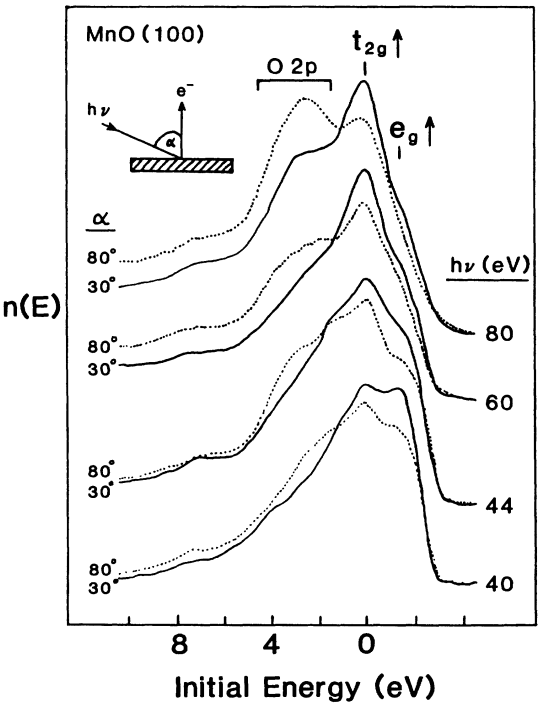

FIG. 4. Normal emission spectra for nearly p polarization ($\alpha = 80°$) and nearly s polarization ($\alpha = 30°$) compared at several photon energies.

It is evident from Fig. 4 that the $e_{g\uparrow}$ emission has a larger intensity relative to the $t_{2g\uparrow}$ emission for the s-polarization geometry and that the O $2p$ region is enhanced for p polarization. This behavior can be interpreted by considering the $3d$ electrons as completely localized and by applying symmetry selection rules. Within an electric dipole approximation, the measured photoemission intensity I is governed by the matrix element between the initial states (ψ_i) and final states (ψ_f) of the system,[32]

$$I = |\langle \psi_f | \mathbf{A}\cdot\mathbf{P} | \psi_i \rangle|^2 , \tag{2}$$

where $\mathbf{A}$ is the polarization vector of the incident light and $\mathbf{P}$ is the momentum operator. For a normal emission geometry, only final states that are totally symmetric about the surface normal can contribute of the photoemission intensity.[33,34] This condition restricts the initial state symmetry to be the same as that of the dipole operator, $\mathbf{A}\cdot\mathbf{P}$, in order to have a nonzero matrix element. It is useful to consider the symmetry of the dipole operator and the initial states with respect to mirror planes of the surface. If $\mathbf{A}$ is parallel (perpendicular) to a mirror plane, the dipole operator is even (odd) and therefore emission will occur only from even (odd) initial states.[35] The application of these selection rules to each of the four mirror planes for a MnO(100) surface [viz., (010), (001), (011), and (0$\bar{1}$1)] and to the orbitals shown in Fig. 2 determine those initial-state orbitals that con contribute to the measured normal emission spectra. For s polarization, $\mathbf{A}$ is parallel to the (010) mirror plane and therefore the initial states $d_{xz}, d_{x^2-y^2}, d_{z^2}, p_x$, and p_z, which have even symmetry with respect to the (010) plane, will give rise to a nonzero matrix element. Similarly, $\mathbf{A}$ is also perpendicular to the (001) mirror plane, so the selection rules also allow emission from the odd d_{xy}, d_{xz}, and p_x orbitals. Finally, for the (011)-type mirror planes, $\mathbf{A}$ can be resolved into parallel and perpendicular components, and symmetry considerations dictate that emission can arise from the $d_{x^2-y^2}$, d_{xy}, d_{z^2}, and p_z initial-state orbitals. Summarizing the selection rules for the s-polarization geometry, each of the Mn $3d$ and O $2p$ initial state orbitals except for d_{xy} and p_y can couple to the final state. Using similar reasoning for the p-polarization geometry, one finds that all of the initial-state orbitals can contribute to the measured photoemission intensity.

These simple symmetry arguments based on atomiclike $3d$ orbitals qualitatively explain the data in Fig. 4. Because emission from the d_{xy} and p_y orbitals is not allowed for s polarization, the $e_{g\uparrow}/t_{2g\uparrow}$ intensity ratio is larger and the O $2p$ emission is smaller than for p polarization. Since the data were not measured under total polarization conditions, only these qualitative intensity comparisons can be made.

C. Off-normal emission

Valence band spectra were also measured with the detector positioned along off-normal directions within the

(001) and (011) mirror planes of the MnO(100) surface. The incident light was chosen to be of mixed *sp* polarization ($\alpha=45°$), thereby allowing transitions from all of the $3d$ initial-state orbitals. To get an estimate for the relative intensities of emission from the Mn $t_{2g\uparrow}$ and $e_{g\uparrow}$ states, the top of the valence band in each spectrum was fitted to the sum of two Gaussian peaks. The results of the measurements for $h\nu=44$ eV are shown in Fig. 5, where the ratio of the areas of the $t_{2g\uparrow}$ and $e_{g\uparrow}$ Gaussian peaks are plotted versus the polar emission angle θ for measurements in each mirror plane.

If the Mn $3d$ electrons in MnO are localized rather than itinerant, the photoemission intensity along off-normal directions should, to first order, contain symmetry information derived from the initial-state $3d$ orbital wave functions. This is evident by considering the form of the transition probability for photoemission [Eq. (2)] evaluated assuming a plane-wave final state $\langle\psi_f| = \exp(i\mathbf{k}\cdot\mathbf{r})$ and hydrogenic wave functions for the $3d$ initial-state orbitals. The initial-state wave functions have the form $|\psi_i\rangle = R(r)Y_{lm}(\theta,\phi)$, where $R(r)$ is the radial part of the wave function and $Y_{lm}(\theta,\phi)$ represents the angular part in terms of spherical harmonics. Making these substitutions into Eq. (2), the photoemission intensity becomes[36]

$$I \propto |\,\mathbf{A}\cdot\mathbf{k}\,|^2\,|F_{nl}(\rho)|^2 Y_{lm}(\theta,\varphi)\delta(E_f-E_i-h\nu)\ , \qquad (3)$$

where $|F_{nl}(\rho)|^2$ is the Fourier transform of the radial part of the wave function. The angular dependence of the emission is contained within the spherical harmonic terms which are easily evaluated for $3d$ orbitals.[37] Going off-normal in the (001) mirror plane, one would expect emission from the d_{z^2}, d_{yz}, and $d_{x^2-y^2}$ orbitals (see Fig. 2)

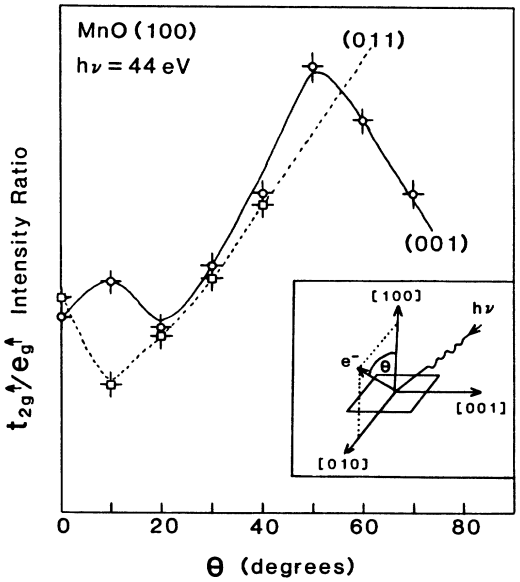

FIG. 5. Ratio of the $t_{2g\uparrow}/e_{g\uparrow}$ emission intensities, determined from angle-resolved EDC's, as the polar angle θ is varied within the (001) and (011) mirror planes of the surface. The inset shows the collection geometry for measurements in the (001) mirror plane.

which have angular dependencies of $3\cos^2\theta-1$, $\sin\theta\cos\theta$, and $\sin^2\theta$, respectively. Within this model, the $t_{2g\uparrow}/e_{g\uparrow}$ intensity ratio should go through a maximum at $\theta=45°$. Likewise, in the (011) mirror plane, the $t_{2g\uparrow}/e_{g\uparrow}$ intensity ratio should exhibit a minimum of $\theta=0°$ and continue to increase for larger angles. This general trend is visible in Fig. 5, but anomalies exist, especially for small angles.

To explain the anomalies in the off-normal emission data, other processes that influence the emission angle of the photoemitted electrons must be considered, namely, refraction of final-state electrons at the surface[32] and initial state[37,38] or final state[39] interference effects. As in LEED experiments, a final-state electron originating from below the surface is refracted by the potential barrier at the surface, where only the parallel component of the electron momentum is conserved. The amount of refraction increases with polar emission angle and depends not only on the size of the potential barrier (V_0) but also on the final-state kinetic energy of the electron (E_f).[32] For uv excitation, this effect can be significant. For example, assuming $V_0=10$ eV and $E_f=40$ eV, an electron directed 45° from the surface normal will be refracted to 52.2° in the vacuum. The net effect of the refraction is to skew the angular distribution of photoelectrons towards larger polar angles. The other structure in the angular distribution may be due to either the coherent interference of initial-state wave functions described by Gadzuk[37,38] or interference of the final-state electrons by multiple scattering.[39]

V. PHOTOEMISSION SATELLITES

In Sec. IV the angle-resolved photoemission data were interpreted within the ligand field picture of completely localized Mn $3d$ electrons. However, satellite peaks are generally visible in both valence-band and core level photoemission spectra from transition-metal compounds which cannot be explained by ligand field theory. These satellites occur at binding energies between 5 and 7 eV above the main lines[40] and have recently been ascribed to multielectron effects involving the transition-metal $3d$ and ligand p states.[13,41–43] The multielectron effects can be present either in the initial or final states. As a final-state effect, it is believed that within the time scale of the photoionization process, the valence levels undergo a relaxation and charge can be transferred from a ligand p to an unoccupied transition-metal $3d$ level to locally screen the photoinduced hole. For core level photoemission from a transition-metal compound in a $3d^n$ ground-state configuration, the main line is assigned to a $\underline{c}3d^{n+1}\underline{L}$ configuration (where $\underline{c}$ and $\underline{L}$ refer to core and ligand holes), which results from the charge transfer screening, whereas the satellite corresponds to a poorly screened $\underline{c}3d^n$ final state. Likewise for valence band emission, the main line and satellite configurations are $3d^n\underline{L}$ and $3d^{n-1}$, respectively. Charge transfer can also be important in the initial (ground) state due to cation-ligand hybridization; this initial-state effect contributes to the $3d^n\underline{L}$ and $3d^{n-1}$ photoemission peaks as well.

Figure 6 displays angle-integrated spectra measured

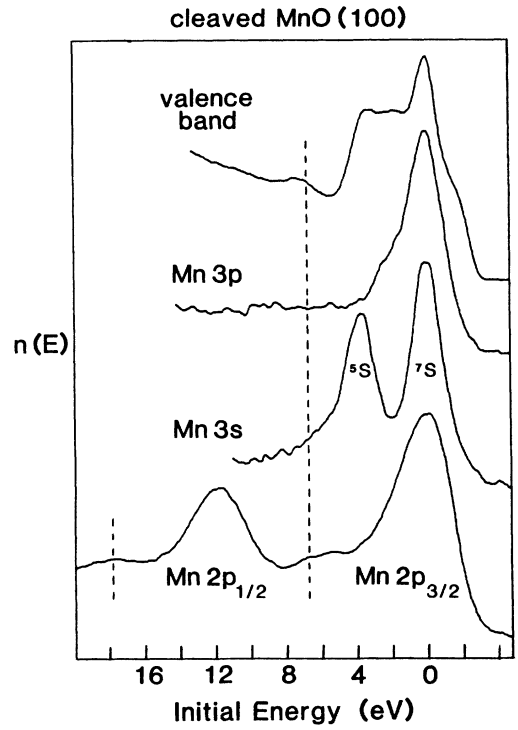

FIG. 6. Angle-integrated photoemission spectra from cleaved MnO(100) showing the satellite location (dashed line) with respect to the main core level and valence-band photoemission peaks. The core and valence spectra were measured with photon energies at 1486.6 eV and 40.8 eV, respectively.

from the Mn $2p$, $3s$, and $3p$ core levels and valence band of cleaved MnO. The satellites are located at binding energies about 7 eV higher than the main lines, and their intensities are very weak compared to those observed from NiO (Ref. 44) and CoO (Ref. 45). The spin-orbit-split Mn $2p$ level has a small satellite associated with each line, but the satellite is scarcely visible in the $3p$ and $3s$ spectra. We believe that the valence band satellite does exist, contrary to a recent claim,[14] but one must be careful to account for the possibility of OH^- contamination on the surface since the 3σ photoemission peak from OH^- coincides with the satellite position.[46]

The multiplet structure in the $3s$ and $3p$ levels arises from multielectron effects. Photoemission from the $3s$ level of a Mn^{2+} compound (^6S initial-state symmetry) can occur via two final states: the ^7S state with the $3s$ electron coupled parallel to the d-shell spin and the ^5S state with the two spins coupled antiparallel. Measurements of this splitting in MnO (Ref. 47) and MnF_2 (Ref. 48) samples have been reported to be on the order of 6 eV, which is about half the value predicted for free ions because of electron correlation.[49] Our measurements of the $3s$ splitting from a cleaved MnO single crystal show both a smaller splitting ($\simeq 3.7$ eV) and narrower peak widths compared to previous measurements. The origin of this effect is unclear and is currently being investigated. In the $3p$ shell, the multiplet splitting gives rise to four closely spaced final states causing a broad $3p$ line shape.

VI. $3p$ ABSORPTION AND RESONANT PHOTOEMISSION

Recently a large amount of effort has been devoted towards understanding the valence band structure of transition-metal and rare-earth compounds from resonant photoemission experiments; the reader is referred to a very comprehensive review by Davis.[40] In the present study this technique has been applied to cleaved MnO samples at the $3p \rightarrow 3d$ absorption threshold, and the resonant enhancement of the Mn $3d$ states in the valence band has been observed for photon energies between $47 \leq h\nu \leq 52$ eV.

The $3p \rightarrow 3d$ resonant photoemission channel becomes operative when the incident photon energy exceeds the Mn $3p$ core excitation threshold. Above this threshold, optical absorption promotes a $3p$ electron into an occupied $3d$ state, and this excited state can decay via a direct recombination process (also known as autoionization) in which a $3d$ electron drops down to fill the $3p$ hole, transferring energy to another $3d$ electron that is ejected into the continuum. In an atomic picture, the configurations can be written $3p^63d^5+h\nu \rightarrow [3p^53d^6]^* \rightarrow 3p^63d^4+e^-$. The final state is indistinguishable from that caused by the direct photoemission process ($3p^63d^5+h\nu \rightarrow 3p^63d^4+e^-$), and the interference between the two channels gives rise to a Fano-type profile for the photoemission intensity as the photon energy is swept through the $3p \rightarrow 3d$ threshold.[40,50–52] Model calculations involving the interaction between the discrete states and the continuum by Davis and Feldkamp[52] yield profiles that agree quite well with measurements from atomic Mn vapor,[53] giving credence to a direct recombination mechanism. In transition-metal compounds, the $3p$ excitation remains localized on the cation site, and a quasiatomic interpretation can be used to describe the resonance behavior. However, multielectron effects and associated satellite peaks in the transition-metal compounds complicate the analysis[54] in comparison to atomic systems.

The resonant enhancement of the $3d$ states in the valence band of MnO is visible in Fig. 7, which shows angle-integrated EDC's measured between $40 \leq h\nu \leq 60$ eV. Each spectrum was corrected to obtain an absolute intensity by taking into account the decay in the synchrotron ring current and the intensity variation of light from the monochromator. The $t_{2g\uparrow}$ and $e_{g\uparrow}$ peaks (corresponding to positions A and B in Fig. 7) appear to undergo an antiresonance between $44 \leq h\nu \leq 52$ eV, while the satellite (position D) resonates. The intensity profile across the $3p$ threshold of a given feature at a binding energy E_b can be observed more quantitatively by measuring CIS spectra, where the photon energy is varied while keeping $(h\nu - E_b)$ constant. However, the problem with this method (which has not been universally recognized) is that a background of inelastic electrons is always included, and the background may have a different resonance behavior from the feature of interest. To avoid this problem, we have generated CIS-type spectra by measuring the peak height (or peak area in the case of the satellite) above an integral inelastic background at a given

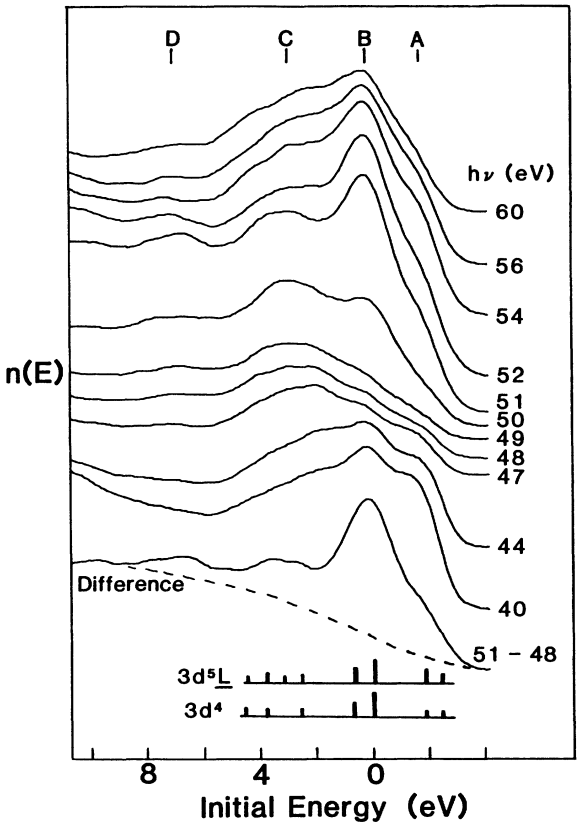

FIG. 7. Angle-integrated EDC's measured from MnO(100) showing resonant enhancement of the $3d$ states. The 51–48 eV difference spectrum is compared to calculated $3d^4$ and $3d^5\underline{L}$ final-state intensities from a CI calculation for a $(MnO_6)^{10-}$ cluster (Ref. 14).

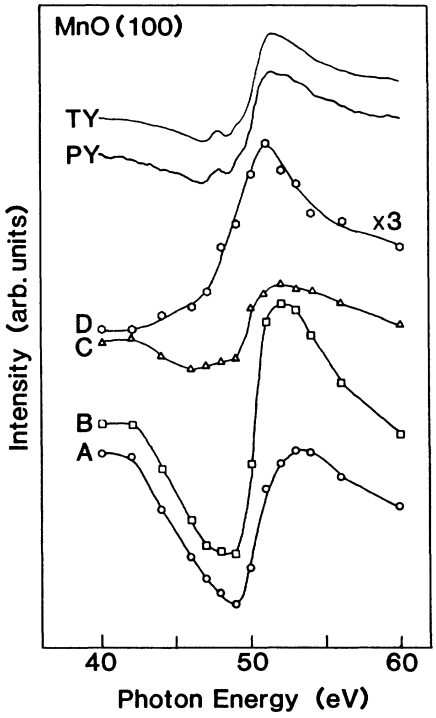

FIG. 8. Total yield (TY) spectrum, partial yield (PY) spectrum, and CIS spectra corresponding to binding energies $A \rightarrow D$ in Fig. 7, across the Mn $3p \rightarrow 3d$ excitation threshold.

binding energy directly from the EDC's. No correction for the decrease in the analyzer transmission with increasing kinetic energy of the photoelectrons[55] was made since the effect is small compared to the resonant behavior.

Figure 8 shows the CIS spectra that correspond to the binding energies $A \rightarrow D$ in Fig. 7. Clearly feature A near the top of the valence band exhibits a strong antiresonance, while the satellites feature D displays a resonance. The profiles at positions B and C appear to consist of both antiresonant and resonant components. Also included in Fig. 8 are the total photoelectron yield (TY) and the partial electron yield (PY) at a kinetic energy of 10 eV obtained from a CFS measurement. The total and partial yield curves exhibit Fano-like profiles that closely resemble the absorption spectrum measured from atomic Mn.[53] The strong increase in intensity near 50 eV is associated with the $(3p^5 3d^6)^6P$ atomic multiplet, while the small peak at 48 eV corresponds to the ^6D multiplet which is prohibited from decaying into a continuum state because of conservation of angular momentum.[40]

In has been demonstrated for other transition-metal compounds[13,42,54,56,57] that the d^{n-1} and $d^n\underline{L}$ final states in the valence band can be distinguished by means of their line shapes in CIS spectra. The d^{n-1} final states tend to exhibit Fano-like resonances, while the $d^n\underline{L}$ final states undergo antiresonant behavior at photon energies immediately proceeding the Fano peak.[54] On this basis, we assign the final states near the top of the valence band in MnO (feature A) to be predominantly of $3d^5\underline{L}$ character and the satellite (feature D) to be primarily $3d^4$-like. Thus MnO can be classified as a charge transfer insulator, like NiO (Refs. 6 and 13) and Fe_xO,[57] in which the insulating gap is of anion $2p \rightarrow$ cation $3d$ in character.

The CIS line shapes corresponding to features B and C in Fig. 7 appear to contain both resonant and antiresonant characteristics. This reflects some hybridization between the Mn $3d$ and O $2p$ states, which leads to an overlap between $3d^4$ and $3d^5\underline{L}$ features in this region of the valence band. The distribution of the $3d$-derived states can be seen more clearly in a difference spectrum taken between spectra that are on and off of the resonance, as shown in Fig. 7; taking the difference removes most of the unhybridized O $2p$ contribution from the valence spectrum. The difference spectrum reveals that the $3d$-derived states extend throughout the valence band and are significantly hybridized with some of the O $2p$ states. The relative intensities of the final states from Fujimori's CI cluster calculation[14] for MnO are shown at the bottom of Fig. 7. An overlap between the $3d^4$ and $3d^5\underline{L}$ final states is borne out in the CI calculation, but it does not predict the existence of the valence band satellite that is observed experimentally.

VII. DISCUSSION

There still remains some controversy as to the validity of localized versus itinerant electron models in describing

the electronic structure of MnO and other transition-metal monoxides. For MnO, our angle-resolved photoemission data have shown that there is an absence of any significant dispersion of the $3d$ states throughout the Brillouin zone, as expected for localized $3d$ electrons. Also, the polarization-dependent and off-normal emission data agree with a localized $3d$ orbital interpretation. Therefore, especially in light of the recent theory for the electronic structure of transition-metal compounds formulated by Zaanen *et al.*,[7] it is becoming clear that a purely itinerant description of the $3d$ electrons in MnO is not correct. For the O $2p$ states in the valence band, the normal emission data suggest the presence of some dispersion, but the broad, complex nature of the spectra precludes obtaining any conclusive evidence on this point. The experimental determination of a small $3d$ bandwidth and possible O $2p$ band dispersion substantiates the assumption used by Zaanen *et al.*[7] in using an Anderson impurity Hamiltonian to calculate the electronic structure of these compounds.

Although our angle-resolved photoemission data suggest that the $3d$ electrons remain localized on the Mn cations, a ligand field picture is not strictly valid; some hybridization with the $2p$ states of neighboring oxygen ligands must be invoked in order to explain the presence of satellite peaks in both the core level and valence band photoemission spectra.[13,41–43] We observe that the magnitudes of the poorly screened satellite peaks are very small compared to the intensities of the screened emission features in MnO, indicating that the time scale for ligand charge transfer screening is much less than the lifetime of the photoinduced hole. The existence of O $2p$–Mn $3d$ hybridization in the valence band can also be inferred from our resonant photoemission measurements across the $3p \rightarrow 3p$ excitation threshold. CIS spectra for states near the upper edge of the valence band were found to exhibit antiresonant behavior, as predicted for hybridized $3d^5\underline{L}$ states,[54] whereas the $3d^4$ states having a Fano-like line shape were found to be concentrated closer to the so-called satellite position. The amount of ligand charge transfer for MnO in the ground state is expected to be small because the Mn^{2+} ion contains a full $3d^{\uparrow}$ configuration,[14] and thus the presence of $3d^5\underline{L}$ states is mainly a final-state effect. In the related compound $MnCl_2$, a Fano-like resonance is observed for all states in the valence band,[58] reflecting a minimal amount of $2p$-$3p$ hybridization and a bonding that is more ionic in nature.

Fujimori's CI cluster calculations for an isolated cation octahedrally coordinated to oxygen ligands clearly demonstrate the importance of O $2p \rightarrow$ Ni $3d$ hybridization in NiO;[13] measurements of the position and intensity of the valence band satellite and the $3p \rightarrow 3d$ resonance behavior have been shown to be in very good agreement with the CI cluster theory. For MnO, the CI cluster calculation[14] shows reasonable agreement with our measurements of the $3d$-derived valence states in that the position of measured intensity maxima correspond to the locations of the predicted final states (see Fig. 7). However, our measurements reveal a valence-band satellite peak which is not predicted by the CI calculations. Based on the resonance behavior in CIS spectra, we identify the final states near the satellite location to be mainly $3d^4$-like and states near the top of the valence band to be primarily $3d^5\underline{L}$ in character. Although an overlap between $3d^4$ and $3d^5\underline{L}$ states is predicted by Fujimori's calculation, our measurements suggest that the degree of hybridization between these states and the p-d charge transfer energy is smaller than the calculation predicts.

In summary, we conclude that MnO is a charge transfer insulator rather than a Mott-Hubbard insulator according to the classification scheme for transition-metal compounds proposed by Zaanen *et al.*[7] This identification is based on the $3d^5\underline{L}$ character for states at the top of the valence band. The difference in energy between the $3d^n\underline{L}$ and $3d^{n-1}$ states in MnO appears to be smaller than for the heavier transition-metal monoxides, suggesting an increase charge transfer energy in going from Ni to Mn in the transition-metal series, as recently postulated.[7] However, all of the transition-metal monoxides appear to be in the regime of charge transfer insulators in which the charge transfer energy is less than the traditional Mott-Hubbard intra-atomic Coulomb energy.

ACKNOWLEDGMENTS

We are grateful to K. E. Smith for many helpful discussions and technical assistance and also to the National Synchrotron Light Source (NSLS) staff, particularly R. F. Garrett, E. Kneedler, M. J. Sagurton, and G. P. Williams, for their assistance and support. This work was sponsored by National Science Foundation Solid State Chemistry Grant Nos. DMR-82-02727 and DMR-87-11423. Research was performed at the National Synchrotron Light Source, Brookhaven National Laboratory, which is supported by the U.S. Department of Energy, Division of Materials Sciences and Division of Chemical Sciences, Contract No. DE-AC02-76CH00016.

*Present address: Laboratory for Surface Science and Technology and Department of Physics, University of Maine, Orono, ME 04469.

[1]N. F. Mott, Proc. Phys. Soc. London, Sect. A **62**, 416 (1949); Philos. Mag. **6**, 287 (1961); J. Hubbard, Proc. Roy. Soc. London, Sect. A **227**, 237 (1964); **281**, 401 (1964).

[2]K. Terakura, A. R. Williams, T. Oguchi, and J. Kübler, Phys. Rev. Lett. **52**, 1830 (1984).

[3]E. J. Ojala and K. Terakura, Phys. Rev. B **33**, 2733 (1986).

[4]S. Hüfner, J. Osterwalder, T. Riesterer, and F. Hullinger, Solid State Commun. **52**, 793 (1984).

[5]J. M. McKay and V. E. Henrich, Phys. Rev. Lett. **53**, 2343 (1984).

[6]G. A. Sawatzky and J. W. Allen, Phys. Rev. Lett. **53**, 2339 (1984).

[7]J. Zaanen, G. A. Sawatzky, and J. W. Allen, Phys. Rev. Lett.

55, 418 (1985); J. Magn. Mater. **54-57**, 607 (1986); J. Zaanen and G. A. Sawatzky, Can. J. Phys. (to be published).
[8]L. F. Mattheiss, Phys. Rev. B **5**, 290 (1972); **5**, 306 (1972).
[9]T. M. Wilson, J. Appl. Phys. **40**, 1588 (1969).
[10]O. K. Anderson, J. K. Skriver, H. Nohl, and B. Johansson, Pure Appl. Chem. **52**, 93 (1980).
[11]T. Oguchi, K. Terakura, and A. R. Williams, Phys. Rev. B **28**, 6443 (1983); J. Appl. Phys. **55**, 2318 (1984); K. Terakura, T. Oguchi, A. R. Williams, and J. Kübler, Phys. Rev. B **30**, 4734 (1984).
[12]J. Hugel and C. Carabatos, Solid State Commun. **60**, 369 (1986).
[13]A. Fujimori, F. Minami, and S. Sugano, Phys. Rev. B **29**, 5225 (1984); A. Fujimori and F. Minami, *ibid.* **30**, 957 (1984).
[14]A. Fujimori, in *Core Level Spectroscopy in Condensed Systems, Springer Series in Solid-State Sciences* (Springer-Verlag, New York, in press).
[15]C. G. Shull, W. A. Strauser, and E. O. Wollan, Phys. Rev. **83**, 333 (1951).
[16]L. Messick, W. C. Walker, and R. Glosser, Surf. Sci. **37**, 267 (1973).
[17]Y. N. Ksendzov, I. L. Korobova, K. K. Sidorin, and G. P. Startsev, Fiz. Tverd. Tela (Leningrad) **18**, 173 (1976) [Sov. Phys.—Solid State **18**, 99 (1976)].
[18]D. R. Huffman, R. L. Wild, and J. Shinmei, Chem. Phys. **50**, 4092 (1969).
[19]D. E. Eastman and J. L. Freeouf, Phys. Rev. Lett. **34**, 395 (1975).
[20]V. G. Bhide and R. H. Dani, Physica **27**, 821 (1961).
[21]M. Prutton, J. A. Walker, M. R. Welton-Cook, R. C. Felton, and J. A. Ramsey, Surf. Sci. **89**, 95 (1979).
[22]J. B. Goodenough, Prog. Solid State Chem. **5**, 145 (1972).
[23]P. S. Bagus, J. L. Freeouf, and D. E. Eastman, Phys. Rev. B **15**, 3661 (1977).
[24]J. Kübler and A. R. Williams, Proceedings of the International Conference on Magnetism, San Francisco, 1985 (unpublished).
[25]See, for example, E. W. Plummer and W. Eberhardt, Adv. Chem. Phys. **46**, 553 (1983), and references therein.
[26]N. B. Brookes, D. S. Law, T. S. Padmore, D. R. Warburton, and G. Thornton, Solid State Commun. **57**, 473 (1986).
[27]K. E. Smith and V. E. Henrich, Phys. Rev. B **38**, 5965 (1988).
[28]K. Siratori, S. Suga, M. Taniguchi, K. Soda, S. Kimura, and A. Yanase, J. Phys. Soc. Jpn. **55**, 690 (1986).
[29]R. J. Lad and V. E. Henrich (unpublished).
[30]H. Kato, T. Ishii, S. Masuda, Y. Harada, T. Miyano, T. Komeda, M. Onchi, and Y. Sakisaka, Phys. Rev. B **32**, 1992 (1985).
[31]K. Naito, A. Kakizaki, T. Komatsubara, H. Sugawara, I. Nagakura, and T. Ishii, J. Phys. Soc. Jpn. **54**, 416 (1985).
[32]M. Scheffler, K. Kambe, and F. Forstmann, Solid State Commun. **25**, 93 (1978).
[33]J. Hermanson, Solid State Commun. **22**, 9 (1977).
[34]W. Eberhardt and F. J. Himpsel, Phys. Rev. B **21**, 5572 (1980).
[35]E. W. Plummer and W. Eberhardt, Phys. Rev. B **20**, 1444 (1979).
[36]E. W. Plummer, in *Interactions on Metal Surfaces,* edited by R. Gomer (Springer-Verlag, New York, 1975).
[37]J. W. Gadzuk, Phys. Rev. B **12**, 5608 (1975).
[38]J. W. Gadzuk, Solid State Commun. **15**, 1011 (1974); Phys. Rev. B **10**, 5030 (1974); Surf. Sci. **53**, 132 (1975).
[39]A. Liebsch, Phys. Rev. Lett. **32**, 1203 (1974); Phys. Rev. B **13**, 544 (1976).
[40]L. C. Davis, J. Appl. Phys. **59**, R25 (1986), and references therein.
[41]S. Larsson, Chem. Phys. Lett. **32**, 401 (1975); **40**, 362 (1976); S. Larsson and M. Braga, *ibid.* **48**, 596 (1977).
[42]G. van der Laan, C. Westra, C. Haas, and G. A. Sawatzky, Phys. Rev. B **23**, 4369 (1981); G. van der Laan, Solid State Commun. **42**, 165 (1982).
[43]B. W. Veal and A. P. Paulikas, Phys. Rev. Lett. **51**, 1995 (1983); Phys. Rev. B **31**, 5399 (1985).
[44]J. M. McKay and V. E. Henrich, Phys. Rev. B **32**, 6764 (1985).
[45]J. L. Mackay and V. E. Henrich (unpublished).
[46]R. J. Lad and V. E. Henrich (unpublished).
[47]C. S. Fadley, D. A. Shirley, A. J. Freeman, P. S. Bagus, and J. V. Mallow, Phys. Rev. Lett. **23**, 1397 (1969); C. S. Fadley and D. A. Shirley, Phys. Rev. A **2**, 1109 (1970).
[48]S. P. Kowalczyk, L. Ley, R. A. Pollak, F. R. McFeely, and D. A. Shirley, Phys. Rev. B **7**, 4009 (1973).
[49]P. S. Bagus, A. J. Freeman, and F. Sasaki, Phys. Rev. Lett. **30**, 850 (1973).
[50]U. Fano, Phys. Rev. **124**, 1866 (1961).
[51]R. E. Dietz, E. G. McRae, Y. Yafet, and C. W. Caldwell, Phys. Rev. Lett. **33**, 1372 (1974).
[52]L. C. Davis and L. A. Feldkamp, Phys. Rev. B **23**, 6239 (1981).
[53]R. Bruhn, E. Schmidt, H. Schröder, and B. Sonntag, Phys. Lett. **90A**, 41 (1982); E. Schmidt, H. Schröder, B. Sonntag, H. Voss, and H. E. Wetzel, J. Phys. B **18**, 79 (1985).
[54]L. C. Davis, Phys. Rev. B **25**, 2912 (1982).
[55]J. Barth, F. Gerken, and C. Kunz, Phys. Rev. B **31**, 2022 (1985).
[56]A. Fujimori, M. Saeki, N. Kimizuka, M. Taniguchi, and S. Suga, Phys. Rev. B **34**, 7318 (1986).
[57]A. Fujimori, N. Kimizuka, M. Taniguchi, and S. Suga, Phys. Rev. B **36**, 6691 (1987).
[58]A. Kakizaki, K. Sugeno, T. Ishii, H Sugawara, I. Nagakura, and S. Shin, Phys. Rev. B **28**, 1026 (1983).